Title
Microclimate and Surface Flux Impact of Utility Scale Solar Installations: A Physical Model

Author
Glasner, Jessica Irene

Publication Date
2020

Peer reviewed|Thesis/dissertation

UNIVERSITY OF CALIFORNIA SAN DIEGO

Microclimate and Surface Flux Impact of Utility Scale Solar Installations: A Physical Model

A thesis submitted in partial satisfaction of the
requirements for the degree
Master of Science

in

Engineering Sciences (Mechanical Engineering)

by

Jessica Irene Glasner

Committee in charge:

Professor Carlos F. M. Coimbra, Chair
Professor Jan Kleissl
Professor Renkun Chen

2020

The thesis of Jessica Irene Glasner is approved, and it is acceptable in quality and form for publication on microfilm and electronically:

Chair

University of California San Diego

2020

DEDICATION

In recognition to all those who have provided direct and indirect guidance throughout my life, allowing me to discover how to be and how not to be, those gentle and those firm lessons and experiences, for shaping the person I am now and as I look forward with vigor to continue evolving:

Carlos F.M. Coimbra, PhD

Aaron Drews, PhD

Erika Peters, PhD

Keith Cunningham

David Lewiston

Josef Mart

JB Straubel

David Larson, PhD

Most importantly, I dedicate this thesis to my father and mother, Jack Boggs Glasner and Patricia Ann MacDonald, for their strengths as parents and weaknesses as humans have made me the grateful and empowered woman I am today.

EPIGRAPH

Remember to look up at the stars and not down at your feet. Try to make sense of what you see and wonder about what makes the Universe exist. Be curious. And however difficult life may seem, there is always something you can do and succeed at.

—Stephen Hawking, PhD

TABLE OF CONTENTS

LIST OF FIGURES

0.1 Nomenclature

u_e : wind speed [m/s]

ε : emissivity [-]

α : absorptivity [-]

ρ : reflectivity [-]

τ : transmissivity [-]

σ : Stefan-Boltzmann constant [W m^{-2} K^{-4}]

T_e : temperature of environment/air [K]

T_s: surface temperature [K]

M : molar mass [g/mol]

RH: relative humidity [-]

h_c: convective heat transfer coefficient [W m^{-2} K^{-1}]

k: thermal conductivity [W m^{-1} K^{-1}]

$\hat{h}_{fg}$: enthalpy of vaporization [J kg^{-1}]

$\dot{m}''$: mass flow rate [kg m^{-2} s^{-1}]

g_m: mass transfer conductance [kg m^{-2} s^{-1}]

T: temperature [K]

L: length [m]

Re: Reynolds number [-]

Pr: Prandtl number [-]

Nu: Nusselt number [-]

Sh: Sherwood number [-]

Sc: Schmidt number [-]

G: irradiance [W m^{-2}]

J: radiosity [W m^{-2}]

q: energy flux [W m^{-2}]

$(\widetilde{\cdot})$: shortwave radiation band

$(\cdot)_g$: ground

$(\cdot)_{\bar{s}}$: surface, averaged

$(\cdot)_p$: panel

$(\cdot)_{p,t}$: panel, top

$(\cdot)_{p,b}$: panel, bottom

$(\cdot)_{np}$: no panel

$(\cdot)_{e}$: environment

$(\cdot)_{s}$: surface

$(\cdot)_{\mathrm{tr}}$: transition

$(\cdot)_{\mathrm{L}}$: lengthscale

$(\cdot)_{\mathrm{rad}}$: radiation

$(\cdot)_{\mathrm{cond}}$: conduction

$(\cdot)_{\mathrm{conv}}$: convection

$(\cdot)_{\mathrm{lat}}$: latent

$(\cdot)_{\mathrm{PV}}$: photovoltaic (PV)

$(\cdot)_{\mathrm{CSP}}$: concentrating solar power (CSP)

where u_e, RH, ε_g, and $T_e \in \mathbf{R}^n$ (i.e. u_e is a n-element real-valued vector). T_s (surface temperature) and $\dot{m}''$ (mass transfer rate) are functions of the aforementioned parameters, also represented as n-element real-valued vectors.

ACKNOWLEDGEMENTS

A special thanks to Professor Carlos F. M. Coimbra for his guidance and support throughout my undergraduate and graduate career at University of California San Diego.

I also thank David Larson, PhD, for his support in the code structure of this physical model and his continued optimism and understanding.

VITA

2014 - 2015	Undergraduate Research Assistant, University of California San Diego
2015	Bachelor of Science in Chemical Engineering, University of California San Diego.
2015 - 2017	Undergraduate Teaching Assistant in Chemical Engineering, University of California San Diego
2015 - 2020	Graduate Research Assistant, University of California San Diego
2020	Master of Science in Engineering Sciences (Aerospace Engineering), University of California San Diego.

FIELDS OF STUDY

Major Field: Engineering Sciences (Aerospace Engineering)

Thermal Sciences, Applied Atmospheric Sciences, and Environmental Engineering

ABSTRACT OF THE THESIS

Microclimate and Surface Flux Impact of Utility Scale Solar Installations: A Physical Model

by

Jessica Irene Glasner

Master of Science in Engineering Sciences (Mechanical Engineering)

University of California San Diego, 2020

Professor Carlos F. M. Coimbra, Chair

Utility-scale solar energy has become a popular solution for the renewable energy market and has proven to drive down the cost of energy by introducing competition to the marketplace, however there remains potential for unforeseen impacts. In recent years, more research has been targeted at exploring the impacts of USSE and its effect on climate conditions - both global with climate simulations [16], [7], [11] and at the local level as a threat to ecosystems [20], [12].

In this model, the local ground temperature and respective mass transfer rates are

simulated under varied conditions, including an open ground-sky interface and ground behavior with a panel overhead. A sensitivity analysis is also performed to assess the impact of ground emissivity, local wind speed, and relative humidity on local conditions. Further, the relative surface fluxes are evaluated to compare the change in albedo effect in the presence of photovoltaic panels, heliostat panels, to an open ground-sky interface.

Ground surface flux depends heavily on radiative heat transfer with no panel overhead, and depends almost completely on convective heat transfer with a panel overhead, showing hundreds of Watts of flux reduced during the daytime. With a panel overhead, ground temperatures are reduced by up to 40 K during the day, due to shading; during the nighttime the panel keeps the ground temperature warmer by up to 20 K due to lack of radiative exchange with the sky. Increased ground temperature during the nighttime can be resolved by rotating the panels perpendicular to the ground surface, though this has an unknown effect on local wind patterns. Mass transfer rates, specifically evaporation, are reduced up to an order of magnitude during the daytime with the presence of a panel overhead the ground surface; nighttime cases, with no intervention such as rotating the panels, show a lack of condensation formation on the ground surface with panels overhead.

The overall surface flux of the panels when compared to the ground is significantly reduced, especially in the heliostat case, where over 1000 W m^{-2} is reflected onto either a collector or back to space in the shortwave portion of the spectrum. PV panels show about 100 W m^{-2} lower surface flux than the open ground. Both panel cases contribute less surface flux to the atmosphere, suggesting lower radiative forcing than the open ground-sky interface.

Introduction

A global surge in renewable energy technologies has taken hold since the 2010s, seeing a five-fold investment in renewables from the 2000s [18]; the benefits and implications are evolving as these deployments unfold. Technology is rapidly improving, particularly in the material science aspect for applications in solar renewable technologies: photovoltaic cells are becoming more diverse in resource material and efficiency, and molten salts are becoming more competitive as a solution to a lack of storage in solar energy. In addition, the National Renewable Energy Laboratory (NREL) in the United States has estimated that the solar energy potential within the USA is capable of providing 400 zetawatt-hours annually (ZWh)[15], hugely exceeding the current electrical generation capacity (22,813 terawatt-hours (TWh) [19].

Due to the footprint of grid-scale solar power solutions in the form of either PV or CSP, this begets a responsibility to evaluate the impact to the surrounding environment and ecosystems. According to Hernandez et al [10], land-atmosphere interactions and climate change associated with USSE are increasing with a need to consider climate feedbacks. Specifically in this model, the presence of a panel overhead the ground surface in an

arid climate, such as the American Southwest, is evaluated at a local scale implementing and heat and mass transfer balance to assess the impact to local ground temperatures and mass transfer rates of the soil. The physical impacts to the energy budget of said systems are effective albedo and surface roughness [10]. A change in albedo directly affects the radiative energy transfer and thereby cooling or warming of the surfaces and air temperature, while changes in surface roughness may impact local wind patterns and directly impact convective transport.

Chapter 1 provides an overview of USSE technologies, specifically PV and CSP, and an introduction to a recently defined phenomena associated with large-scale solar installations, the "photovoltaic heat island effect" (PVHI).

This model quantifies the impact to local ground temperature and mass flux in ambient conditions compared to the presence of a panel overhead with an energy balance. Surface fluxes are also evaluated. The details of the model are covered in Chapter 2.

In Chapter 3, the results of ground temperature and mass flux at the ground surface are discussed as a function of air temperature, T_e, ground emissivity, ε_g, wind speed, u_e, and relative humidity, RH, under normal clear skies during the daytime and nighttime, with and without a panel overhead the ground. Ground surface flux, PV panel, and heliostat panel surface fluxes are compared as well at fixed ε_g, u_e, and RH.

Chapter 1

Utility-Scale Solar Energy

Leading the US solar market since 2012, utility-scale solar is defined as any ground-mounted, greater than 1 MW_{AC}, solar project, and includes photovoltaic (PV), concentrated photovoltaic (CPV), and concentrated solar-thermal power (CSP) [21]. Conversely, local or residential systems are referred to as "distributed". With renewable technologies, namely solar, breaking into the energy market and rapidly growing over the last decade, grid operators are responsible for reconfiguring power distribution, trying to manage fluctuating power sources and a shifted diurnal peak demand window, intensified by distributed and utility-scale solar. Utility-scale solar coupled with storage provides a solution for the needed stability of grid operation, using renewable sources [8]. Total energy consumption in 2019 for the US was 29.4 PWh, with utility scale solar (PV and CSP) generating 72.2 GWh [21]. The American southwest boasts the highest density of installed utility-scale solar due to its exceptionally high irradiance compared to the rest of the country, and has installed over 14 GW combined nameplate capacity [21].

This rapidly expanding technology has direct impact to land use requirements, with the footprint of USSE being 9 acres/MW on average, total land use, which includes the entire enclosed area of a site. Direct land use, which includes the equipment only, PV panels, heliostats, and CSP towers, of USSE applications account for between 70-85% of the total land use. [19] With over 75% of USSE plants generating between 1-5MW, this suggests that most installations are no larger in footprint than 45 acres, however, regarding newer plants being on the order of 250MW, we can see up to 2250 acres for a single facility [21]. Predictions suggest that PV deployment will increase in scale up to multiples of terawatts, which can have an effect on climate change behavior [16]; namely, radiative forcing due to change of land use given the presence of either dark (colored) PV panels or highly reflective mirrors (heliostats).

Additionally, since many facilities are developed on public lands, impact to the local ecosystem has become relevant. For example, construction of Ivanpah Solar Power Facitlity was halted for two months to investigate and introduce restrictions in order to protect the threatened desert tortoise [19].

Investigations of impacts of large-scale solar installation and operation have found mostly beneficial compared to fossil fuel generation in areas such as human health and well-being, wildlife and habitat, and global reduced CO_2 emissions. However, an area lacking clarity is local climate impact, specifically modifications to surface albedo [20]. Microclimate impacts, specifically in the Southwestern US, are currently speculation in most cases, estimating a change in surface albedo between 30-56%, impacts local temperatures, evapotranspiration, and precipitation patterns [12]. The magnitude of the impact

is currently unresolved.

1.1 PV Power Plants

Photovoltaics have been widely implemented since the 2010's, having proven to be more efficient for local power generation than concentrated solar power, as it can generate electricity under both direct and diffuse radiation, and the cost of tradiational c-Si panels has dropped due to improvements in technology and manufacturing. PV is also robust in its reliability aspect, with few or no moving parts [14]. A challenge in large-scale PV has to do with footprint: consideration must be given to shading effects as the reduction in irradiance on the panel drastically reduces power output; optimization of maximizing power density per acre and proper spacing is a fundamental design consideration for large-scale projects.

Utility-scale power generation has increased 70x from PV alone over the last decade, from generating just over one GW in 2011 to 69 GW in 2019 [21]. Although the US reports more than 2,500 utility-scale solar PV facilities, most are relatively small and account for 2.5% of the USSE generating capacity and 1.7% of the annual electricity generation, as of November 2018 [21].

According a most recent NREL report, PV USSE occupies 8.4 acres/MW on average, total land use, and up to 6.7 acres/MW for direct land use. In one scenario, it is estimated that 13.6 million acres, or about 0.6% of total land use in the US would be required to supply all end-use electricity with PV as the only source [19].

Though data and research is lacking, there is concern regarding the impact of USSE installations to some desert wildlife species, most specifically the Aggasiz tortoise [12]. Additionally, the construction and commissioning of USSE PV installations present impact to the following: dust generation and suppression, increased soil erosion and compaction, habitat fragmentation, and microclimate effects due to localized heating [12].

Finally and potentially most important to quantitatively evaluate, is that photovoltaic panels alter the local energy balance, such that the surface albedo is directly modified to be substantially lower in the shortwave radiative spectrum, leading to reduced energy reflection back to space. Further, these panels re-emit radiation in the infrared (IR) range of the electromagnetic spectrum, introducing localized heating.

1.2 CSP Power Plants

Though concentrated solar power does not match the scale of photovolatics in USSE in power generation, it provides more energy per unit of capacity given the storage capability in conjunction with solar power generation [14]. The complication of moving parts, pumps, and working fluids make this technology less robust, however it does offer more jobs. Traditional working fluids include high viscosity oil in parabolic trough, and molten salts, with tower applications gaining popularity due to higher fluid temperatures and shorter distances of travel for heated fluids.

CSP technology for USSE hasn't grown quite as rapidly as PV, seeing an increase from just under a GW in 2010 to over three GW in 2019, likely owing to higher capital

costs than traditional PV.

CSP USSE takes up 10 acres/MW on average, total land use, which includes the entire enclosed area of a site. Direct land use, which includes the equipment such as, heliostats, CSP towers, and generators occupy 7.7 acres/MW on average [19]. Limited data shows that the land-use requirement increases about 5-6 acres/MW-year for every additional 5 hours of energy storage [14].

The environmental impact of CSP installations predominantly concern that of water usage, soil erosion, and local wildlife (birds). Water consumption is necessary for cleaning the mirrors and wet cooling, which consumes 3.07 m^3/MWh [10]. The mortality rate observed at one facility in a study over 40 weeks shows 1.9-2.2 individual bird deaths per week, with 81% due to collision with site infrastructure, and 19% due to burning while crossing the path of the concentrated beam reflected from the heliostat to the collector tower [10]. Lastly, the presence of the heliostat panels reduces soil erosion rate, potentially a desirable effect [22].

The presence of heliostat panels suggests a net cooling effect for an area given that a majority of the incoming shortwave radiation is either reflected and concentrated onto a collector, or reflected back to space.

1.3 Photovoltaic Heat Island Effect

A heat island effect is most commonly observed in urban areas, and put simply, refers to the change in local temperatures due to a change of the topography of an area,

resulting in increased local temperatures when compared to the natural habitat preceding the human development. Surface heat islands tend to present the strongest during the day, while atmospheric heat islands present in the nighttime, as the local radiative energy exchange is altered, sometimes drastically [17].

Extracting the concept of an urban heat island and primarily focusing on the American Southwest and its relevant topography, most of the terrain wherein USSE PV applications are installed is predominantly desert, due to the high irradiation and clear day frequency, which introduces the idea of a photovoltaic heat island effect (PVHI).

The optical properties of traditional PV panels are such that incoming shortwave radiation is converted to electricity, at around 20% efficiency, with the remaining energy being rejected as waste heat, locally. As the scale of PV panels increases, it has been observed that local heating effects are measurable.

In 2013, a comprehensive study reported results of an average increase in local air temperature within a large-scale PV farm to be 1.9°C above surrounding ambient, with measurable decrease to ambient air temperature up to 800 m away from the edge of the solar farm perimeter [9]. In 2016, as separate study reported results that temperatures over a 1 MW PV power facility when compared to the surrounding desert terrain were consistently 3-4°C warmer during the nighttime [6]. This confirms an objectively measurable impact to local air temperature in the presence of large-scale PV solar arrays. Considering large-scale CSP installations, it is reasonably assumed that there may be a net cooling effect due to the concentration and reflection of incoming shortwave radiation.

Though it is outside the scope of this model, it is worth noting that the local air

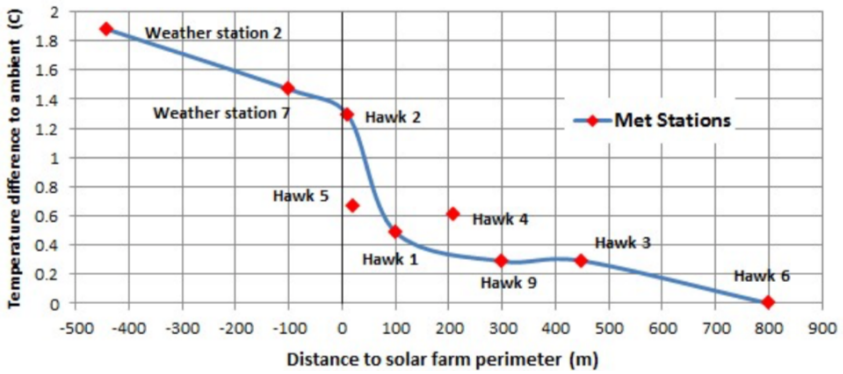

Figure 1.1: Air temperature difference as a function of distance from the perimeter of the solar farm. Negative distances indicate locations within the solar farm. [9]

temperature is also impacted in the presence of a large-scale PV array, as shown in 1.1 [9]. This is likely due to panels releasing energy in the longwave portion of the spectrum and the inhibition of radiative exchange of the ground with the sky, specifically at night. Similar behavior of increased local air temperature was found independent of Fthenakis' findings, by Gafford [6].

The impact to the ground temperature and local mass transfer rates in the presence of panels over the ground surface have yet to be quantitatively evaluated, lending to the motivation of this model and paper.

Chapter 2

Model

This model is built upon first principles of terrestrial dynamics under the influence of radiative energy; incoming radiation is balanced by itself, conductive, convective, and latent heat transfer of surfaces. Participating media is not considered, nor is incident or surface geometry variations. Considering a source of radiation (Sun), the steady-state surface temperature and mass flux will be observed for the ground open to the sky, daytime and nighttime, and with a photovoltaic panel overhead, and a heliostat overhead. The surface temperature of the PV panel or heliostat will influence the ground temperature, but moreso it is expected that the ground temperature during the day will be lower due to shading, while nighttime may be warmer as the ground will be obscured from exchanging energy with the sky. The relative mass transfer rates will be investigated with a primary interest in condensation effects due to covering the ground from the night sky. A sensitivity analysis is done on the following variables to establish their impact on local mass transfer rates:

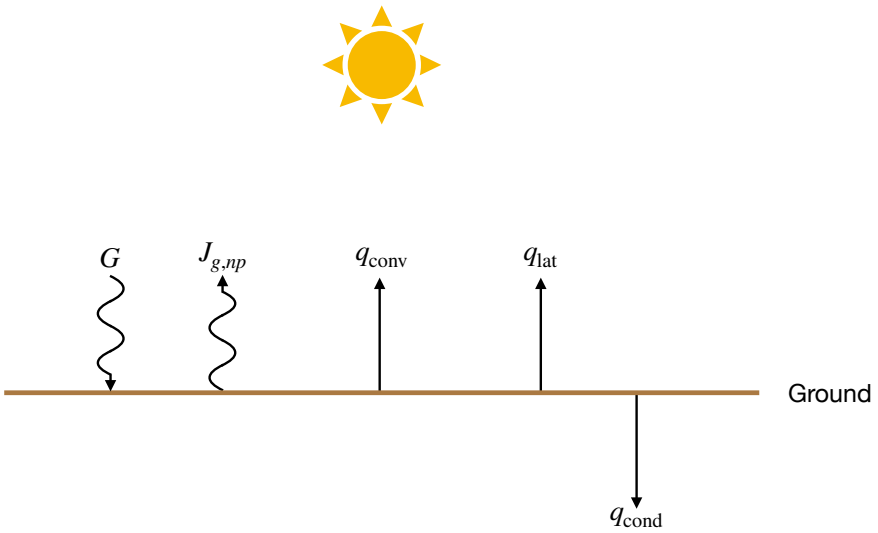

Figure 2.1: Energy Balance, no panel overhead.

- wind speed, u_e [m/s]
- air temperature, T_e [K]
- ground emissivity, ε_g [-]
- relative humidity, RH [-]

Figures 2.1 and 2.2 represent surface energy balances and relative modes of energy transfer.

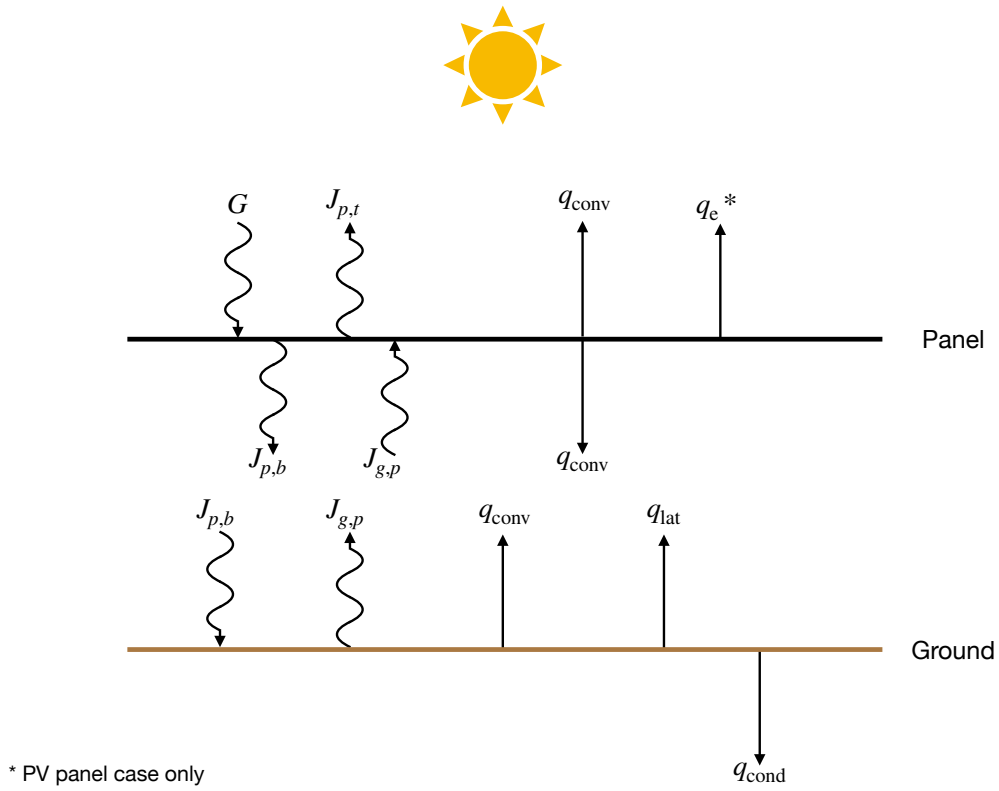

Figure 2.2: Energy Balance, with panel overhead.

2.1 Overall Energy Balances

Consider a control volume including the Earth, the Earth's atmosphere, and the Sun as a source of energy in the form of radiation, and n-surfaces below the Sun, that are parallel to the ground (including the ground surface) normal to incoming radiation from the Sun. The generalized energy balance, at thermal equilibrium is:

$$0 = \text{In - Out} = q_{\text{net}} = q_{\text{rad}} - q_{\text{conv}} - q_{\text{cond}} - q_{\text{lat}} \tag{2.1}$$

Where, the basic expressions for each term are as such:

$$q_{\text{rad}} = G - J \tag{2.2}$$

$$q_{\text{conv}} = h_c(T_s - T_e) \tag{2.3}$$

$$q_{\text{cond}} = -k(T_s - T_{\bar{s}}) \tag{2.4}$$

$$q_{\text{latent}} = \dot{m}''\hat{h}_{fg} \tag{2.5}$$

Where G and J represent the radiative energy transfer, with a T^4 dependency. The remaining terms represent convective heat transfer, latent heat transfer (simultaneous heat and mass transfer), and conductive heat transfer, respective of 2.1, and have a linear dependency on surface temperature, T. It should be noted that J, radiosity, can represent an incoming source of energy for one surface, while it is outgoing energy for a different surface.

Materials have varying surface properties that dictate the way they interact with radiation, the optical properties are explained in further detail in Section 2.2.1. The sur-

face fluxes are dependent on surface temperature, which is the unknown variable in the surface energy balances. Solving a non-linear system of equations, with known irradiance and dependent parameters dictate the surface temperature.

Parameters that will affect surface temperature are as follows:

- optical properties: α, ρ, and ε, which are all are material properties
- heat transfer coefficient, h_c, depends on wind speed, u_e
- thermal conductivity, k, is a material property
- mass flow rate, $\dot{m}''$, depends on a concentration gradient and a temperature differential between the ground surface and ambient air

The entire system, with no panel overhead and the ground exposed to the sky, has the following surface energy balance:

$$\begin{aligned} 0 &= q_g \\ &= \widetilde{\alpha}_g \widetilde{G} + \alpha_g G_{\text{LW}} - J_g - h_{c,g}(T_g - T_e) - (-k(T_g - T_{\bar{g}})) - \dot{m}'' \hat{h}_{fg} \end{aligned}$$

The entire system, at thermal equilibrium, with a panel overhead the ground (n = 2 surfaces), has the following surface energy balance:

$$0 = q_p + q_g$$

Where,

$$
\begin{aligned}
0 &= q_p \\
&= \widetilde{\alpha}_{p,t}\widetilde{G} + \alpha_{p,t}G_{\mathrm{LW}} + \alpha_{p,b}J_g - J_{p,t} - J_{p,b} - 2(h_{c,p}(T_p - T_e)) \\
0 &= q_g \\
&= \alpha_g J_{p,b} - J_g - h_{c,g}(T_g - T_e) - (-k(T_g - T_{\bar{g}})) - \dot{m}''\hat{h}_{fg}
\end{aligned}
$$

Each heat transfer term is expanded and defined in the following sections.

2.2 Radiative Heat Transfer

A dual-band radiation model is implemented, separating shortwave and longwave to capture the varying optical properties of the surfaces given different ranges of the wavelength spectrum. Energy balances will refer to shortwave irradiance, captured by the first band of the model, as $\widetilde{G}$, while longwave irradiance, captured by the second band, is referred to as G_{LW}, including the longwave from solar and the sky:

$$G_{\mathrm{LW}} = G_{\mathrm{Sun,\ LW}} + J_{\mathrm{sky}} \tag{2.6}$$

and overall irradiance, G, which is broken down into 2 bands is:

$$G = G_{\mathrm{LW}} + \widetilde{G} \tag{2.7}$$

The longwave irradiance from the sky has been calculated modeling the sky as a blackbody using the recalibrated Brunt model for sky emissivity, respective of daytime vs nighttime [13]:

$$J_{\text{sky}} = \varepsilon_{\text{sky}} \sigma T_e^4 \tag{2.8}$$

and the emissivity of the sky is:

$$\text{Daytime clear-sky model} : \varepsilon_{\text{sky}} = 0.598 + 0.057\sqrt{P_w} \tag{2.9}$$

$$\text{Nighttime clear-sky model} : \varepsilon_{\text{sky}} = 0.633 + 0.057\sqrt{P_w} \tag{2.10}$$

The simulation run with PV panels as the surface over the ground must account for losses due to electricity conversion during the daytime, at some efficiency, η_p:

$$q_e = \eta_p \widetilde{G}(1 - \widetilde{\rho_{p,t}}) \quad [\text{W m}^{-2}] \tag{2.11}$$

The efficiency used may be found in 2.6.

2.2.1 Optical Properties

Real surfaces have spectrally resolved optical properties: absorptance (absorptivity) α, reflectance (reflectivity) ρ, transmittance (transmissivity) τ, and emittance (emissivity)

ε, all ranging from 0 to 1 and dependent on temperature. The fraction of radiation absorbed by a real surface normalized by the absorptance of a perfectly black surface is given by α. Similarly, ρ is the fraction of radiation reflected by a surface, and τ is the fraction transmitted. Given these definitions, we may introduce the following:

$$\alpha + \rho + \tau = 1 \tag{2.12}$$

therefore, all radiation incident on a surface may be absorbed, transmitted, and/or reflected. In this application, there is no transmittance observed for any surface, so 2.12 becomes:

$$\alpha + \rho = 1 \tag{2.13}$$

Emissivity as not only temperature dependent, but strongly tied to surface conditions, therefore it is not captured by the above equation. Emissivity represents the fraction of emissive power of a real surface of that if it were a perfect blackbody or perfect emitter. A value of $\varepsilon = 1$ represents a blackbody, and according to Kirchoff's law for a body at thermal equilibrium, a grey body is represented by:

$$\alpha = \varepsilon \tag{2.14}$$

Specific values used for the optical properties can be found in 2.6.

2.2.2 Radiosity Expressions

J is radiosity of a given surface and $J = \varepsilon E_B + \rho G + \tau G$, and E_B is the blackbody emission of a surface.

The radiosity term, J, expands as follows for all surfaces in the system:

The radiosity of the ground, with no panel overhead:

$$J_{g,np} = \varepsilon_g \sigma T_g^4 + \widetilde{\rho_g} \widetilde{G} + \rho_g G_{\mathrm{LW}} \tag{2.15}$$

The radiosity of the ground, with a panel overhead (same for PV or heliostat, only the optical properties change):

$$J_{g,p} = \frac{1}{1 - \rho_{p,b}\rho_g} \left[\varepsilon_g \sigma T_g^4 + \rho_g \varepsilon_{p,b} \sigma T_p^4\right] \tag{2.16}$$

The radiosity expression for the top of the panel (same for PV or heliostat, only optical properties change):

$$J_{p,t} = \varepsilon_p \sigma T_p^4 + \widetilde{\rho_{p,t}} \widetilde{G} + \rho_{p,t} G_{\mathrm{LW}} \tag{2.17}$$

The radiosity of the bottom of the panel (same for PV or heliostat, only the optical properties change):

$$J_{p,b} = \varepsilon_p \sigma T_p^4 + \frac{\rho_{p,b}}{1 - \rho_{p,b}\rho_g} \left[\varepsilon_g \sigma T_g^4 + \rho_g \varepsilon_{p,b} \sigma T_p^4\right] \tag{2.18}$$

2.3 Convective Heat Transfer

In general, the convective heat flux for a given surface, s, per unit area, is shown by *Newton's Law of Cooling*:

$$q_s = h_c(T_s - T_e) \quad [\text{W m}^{-2}] \tag{2.19}$$

Convective heat transfer respective of each surface is represented by 2.3, with the appropriate surface (panel or ground) subsitituted for T_s.

2.4 Conductive Heat Transfer

The general heat conduction energy balance is based on Fourier's law of conduction:

$$\mathbf{q_s} = -k\nabla T \quad [\text{W m}^{-2}] \tag{2.20}$$

where $\mathbf{q_s}$ is the conduction heat flux vector and ∇T is the gradient of a scalar temperature field. Taking 2.20 and assuming steady-state, one-dimensional conduction, we have:

$$q_s = -k(T_s - T_{\bar{s}})$$

which is the form of conductive heat transfer observed in this model. Specifics on values used for thermal conductivity, k and $T_{\bar{s}}$ (the average ground temperature) can be found in 2.6.

2.5 Simultaneous Heat and Mass Transfer

Latent heat transfer will be evaluated at the ground, for the conditions with and without a panel overhead. Determination of the mass transfer rate, $\dot{m}''$, is required. When $\dot{m}''$ is multiplied the latent heat of vaporization of water, $\hat{h}_{fg}$ which is a function of temperature and pressure, the equation yields the latent heat transfer associated with mass transfer, per unit area:

$$q_{\text{lat}} = \dot{m}''\hat{h}_{fg} \quad [\text{W m}^{-2}] \tag{2.21}$$

where,

$$\dot{m}'' = g_{m,1}(m_{1,s} \; - \; m_{1,e}) \quad [\text{kg m}^{-2}\ \text{s}^{-1}] \tag{2.22}$$

and,

$$\begin{aligned} g_{m,1} &= \frac{\mu_{\text{air}}\ \text{Sh}_L}{L\ \text{Sc}} \\ m_{1,s} &= \frac{M_1}{M_{\text{air}}}\ \frac{P_{\text{sat}}(T_s)}{P_{\text{tot}}} \\ m_{1,e} &= \frac{M_1}{M_{\text{air}}}\ \frac{\text{RH}_e P_{\text{sat}}(T_e)}{P_{\text{tot}}} \end{aligned} \tag{2.23}$$

The subscript '1' represents the constituent, water, $g_{m,1}$ is the mass conductance as found by the Chilton-Colburn analogy [15], wherein the Sherwood number, Sh, is analogous to the Nusselt number, Nu. $m_{1,s}$ and $m_{1,e}$ are the mass fractions at the surface and at the environment, respectively. RH_e is the relative humidity away from the surface of

evaporation (or condensation), and will be referred to as RH. P_{sat} is the saturation vapor pressure of water at a given air pressure and temperature and is calculated with the improved Magnus form approximation [1], and P_{tot} is the total air pressure in [Pa]. Sh is the Sherwood number and Sc is the Schmidt number.

2.6 Model Parameters

2.6.1 Cases/Scenarios

All cases were evaluated with no panel over the ground surface, with a PV panel overhead, and a heliostat overhead for a total of 18 cases, see 2.1. The model was run for a the open ground-sky interface, a PV panel overhead and a heliostat overhead; the impact to the ground temperature and thereby mass transfer rate was unaffected by the type of panel overhead, despite almost opposite optical properties and losses due to electricity conversion of the PV panel. PV panel optical properties have been used for all results unless figure states 'heliostat'. Additionally, thermal conduction was neglected for the panel, as a sensitivity analysis yielded the same surface temperature with or without conduction for the panel; radiative and convective heating and cooling most drastically dictate the panel temperature, as discussed in 3.

The variables mass transfer rate, $\dot{m}''$, and the ground temperature, T_g, were both simultaneously solved from surface energy balances. The remaining variables were set to a fixed range, see 2.2 for details. Physical constants used in energy balance equations may be found in 2.4. Note that in 2.1, all cases are listed as if surface flux, q_s, is the

only parameter evaluated, however, T_g and $\dot{m}''$ are both functions of surface flux, so their behavior is also reported and discussed in 3.

Table 2.1: Simulation Scenarios

Case/Scenario	**1**	**2**	**3**
Daytime	$q_s(T_e, \varepsilon_g)$	$q_s(T_e, u_e)$	$q_s(T_e, \mathrm{RH})$
Nighttime	$q_s(T_e, \varepsilon_g)$	$q_s(T_e, u_e)$	$q_s(T_e, \mathrm{RH})$

For each case of varied parameter ε_g, u_e, and RH, while one is varied, the other two are held constant at the following, where applicable: $\varepsilon_g = 0.3$, $u_e = 3.25$ m/s, and RH = 0.3.

2.6.2 Radiation

The standard terrestrial solar spectral irradiance distribution used for this model was generated by several sources including the PV industry, the American Society for Testing and Materials, Government, and laboratories and compiled into one document. [3] The two spectra are classified as AM = 0 or AM = 1.5, of which AM = 1.5 was used. AM of 1.5 best represents radiation at the Earth's surface after absorption and scattering in the upper atmosphere, while AM of 0 is applicable to the top of the atmosphere. Motion

Table 2.2: Varied Parameter Ranges

Variable	$\varepsilon_g[-]$	u_e [m/s]	RH[−]	T_e [K]
Range	0.1 - 1	1 - 10	0.1 - 1	275 - 310

Table 2.3: Optical properties

Optical Parameter	$\widetilde{\alpha}$	$\widetilde{\rho}$	α	ρ	ε
PV panel, top	0.9	0.1	0.9	0.1	0.9
PV panel, bottom	-	-	0.9	0.1	0.9
heliostat, top	0.15	0.85	0.1	0.9	0.1
heliostat, bottom	-	-	0.1	0.9	0.1
ground	0.7	0.3	0.9	0.1	-

of the Sun, declination, azimuth, and elevation angles, solar time, and the Sun's position are all factors that greatly influence the irradiance incident on the Earth's surface in a dynamic model. For purposes of a preliminary estimation, these factors have been ignored in this model, and the irradiance at the surface in question will be considered direct and normal; this will assume that all irradiance is at a maximum intensity, which will be result in the highest temperature possible for the surfaces. We can consider this model a representation of a maximized benefit evaluation.

2.6.3 Convection

Convective heat transfer is found per eqn. 2.19, with the locally averaged heat transfer coefficient, $\overline{h_c}$:

$$\overline{h_c} = \frac{\overline{\mathrm{Nu}}\, k}{L} \tag{2.24}$$

Table 2.4: Physical Constants

Physical Constant	Value	[Units]
σ	5.67^{-8}	W m^{-2} K^{-4}
$\hat{h}_{fg}$	2.5^{6}	J kg^{-1}
ν_{air}	15.66^{-6}	m^2 s^{-1}
μ_{air}	18.43^{-6}	kg m $^{-1}$ s $^{-1}$
k_g	1.6 [4]	W m^{-1} K^{-1}
M_{H_2O}	18.02	g mol $^{-1}$
M_{air}	28.84	g mol $^{-1}$
P_{tot}	101325	Pa
η_{PV}	0.17	-
$T_{\overline{g}}$	295 [5]	K
Sc	0.61 [15]	-
Pr	0.69 [15]	-
Re_{tr}	5^{5} [15]	-

For this model, the surface of the panel or heliostat, and the ground are treated as a flat plate, with $\mathrm{Re_L} > 10^5$, using the following convection correlation: [15]

$$\overline{\mathrm{Nu}} = 0.664\mathrm{Re}_{\mathrm{tr}}^{\frac{1}{2}}\ \mathrm{Pr}^{\frac{1}{3}} + 0.036\mathrm{Re}_{\mathrm{L}}^{0.8}\mathrm{Pr}^{0.43}\left[1 - \left(\frac{\mathrm{Re_{tr}}}{\mathrm{Re_L}}\right)^{0.8}\right] \tag{2.25}$$

Where,

$$\mathrm{Re_L} = \frac{u_e L}{\nu_{air}}$$
$$\mathrm{Pr} = \frac{\nu}{\alpha}$$
$$\overline{\mathrm{Nu}} = \frac{\overline{h}_c L}{k}$$

$\overline{\mathrm{Nu}}$ is the locally averaged Nusselt number. Given that h_c is a function of Nu, which is a function of windspeed, u_e, it is iteratively recalculated based on 2.25 for each wind speed scenario.

2.6.4 Conduction

One dimensional, steady-state conduction is observed with the thermal conductivity, k, as shown in 2.4, used in eqn. 2.20. The average temperature of the ground, $T_{\bar{g}}$, for the Mojave Desert is used from [5] and can also be found in 2.4; the length scale of the average ground temperature is set to 0.5 m.

2.6.5 Simulatenous Heat and Mass Transfer

Low mass transfer theory is observed in this model; modeling high mass transfer rates showed no significant difference at the relative surface temperatures and thereby evaporation and condensation rates. Given that g_m is a function of Sh, which is a function of windspeed, u_e, it is iteratively recalculated based on 2.26 for each wind speed scenario.

$$\overline{\mathrm{Sh}} = 0.664\mathrm{Re}_{\mathrm{tr}}^{\frac{1}{2}}\ \mathrm{Sc}^{\frac{1}{3}} + 0.036\mathrm{Re}_{\mathrm{L}}^{0.8}\mathrm{Sc}^{0.43}\left[1 - \left(\frac{\mathrm{Re}_{\mathrm{tr}}}{\mathrm{Re}_{\mathrm{L}}}\right)^{0.8}\right] \tag{2.26}$$

Regarding the calculation of mass transfer rate, $\dot{m}''$, the mass conductance, g_m, is divided by 5 to reflect a "correction factor" as the mass transfer interface is not an open air-water interface; there is resistance evaporation/condensation due to ground surface variations and properties. The value of 5 is chosen from the Bowen ratio, wherein an arid climate is valued at 5-6. The Bowen ratio is the rate of sensible to latent heat flux of Earth's surface into the air. [2]

Chapter 3

Results and Discussion

The presence of a panel overhead the ground surface collapses the behavior spread of the ground conditions regarding temperature and mass transfer rate, compared to open exposure to the sky, regardless of daytime or nighttime. During the daytime, this may be seen as a benefit, as it keeps the ground temperature lower and reduces evaporation rate. However, during the nighttime, the mass transfer rate is higher at the ground surface given the presence of the panel overhead, as it disallows radiative cooling with the sky, which makes the mass transfer rates higher than the cases without the panel overhead. The inhibition of radiative cooling of the ground may be avoided by rotating the panels (where possible) to be perpendicular to the ground surface during nighttime conditions. There is a net reduction in mass transfer rate with panels overhead.

The existence of a heat island effect due to the presence of the panels, does appear consistent, in that the ground temperature remains warmer during the nighttime, thus displaying higher evaporation rates than without panels present. From a quantitative

perspective, considering the extremes, the difference in ground temperature given the presence of a panel overhead is as high as +10-15°C. Due to this wide variation, a sensitivity analysis is also performed to evaluate extremes and reasonable expected scenarios, see 3.4, 3.5 in this section and 3.9, 3.10 in the Appendix.

The sensitivity analysis suggests that ground emissivity is the most impactful parameter on ground temperature and mass transfer rates specifically with no panel overhead, with low emissivities causing the highest evaporation rates, due to the surface's impaired ability to radiatively cool, thus compensating with latent heat transfer. Wind speed has a similarly high impact on mass transfer rate, with the highest wind speeds generating the highest mass transfer rates, due to increased convection driving the concentration gradient. In the case of the panel overhead, dependence on ground emissivity becomes almost irrelevant; wind speed and relative humidity become the most influential variables affecting mass flux at the ground surface, which both directly affect the concentration gradient.

Notable results of the simulations have shown the following, which will be discussed in further detail in this section; addtional figures may be found in the Appendix:

- T_g monotonically increases with T_e under all conditions
- Radiation dominates T_g behavior for open ground-sky interface
- Convection dominates T_g behavior with panel overhead
- Panels overhead the ground surface cause $\mathrm{T}_{g,p} < T_{g,np}$ during the daytime
- Panels overhead the ground surface cause $\mathrm{T}_{g,p} > T_{g,np}$ during the nighttime

- $\dot{m}''$ monotonically increases with T_g during the daytime
- $\dot{m}''$ monotonically increases with T_g during the nighttime, except in cases where RH and $\varepsilon_g > 0.6$
- Net surface flux of panels is lower than open ground-sky interface

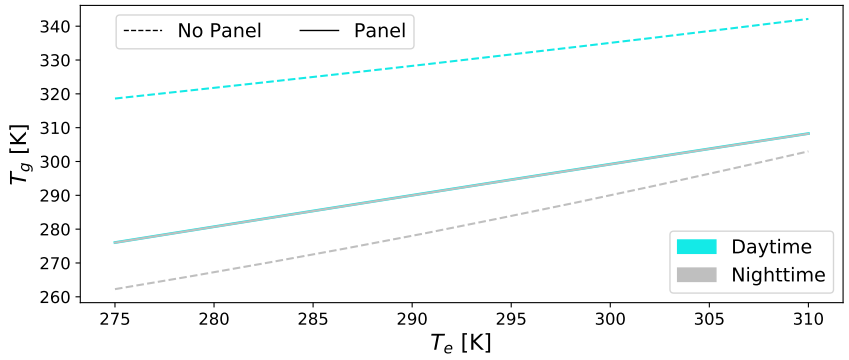

Figure 3.1: Ground surface temperature, T_g, as a function of air temperature, T_e, with and without a panel overhead, daytime and nighttime, RH = 0.3, u_e = 3.25 m/s, and ε_g = 0.3.

Based on the findings shown in 3.1 and as expected, T_g increases with T_e. $T_g(T_e)$ under all varied conditions may be found in the Appendix, Figure 3.8. The presence of the panel overhead the ground surface has a significant impact to ground surface temperature, T_g; during the daytime the panel keeps the ground substantially cooler due to shading, but disallows radiative exchange with the sky during the nighttime, keeping the ground warmer than the case with no panel overhead. The panel overhead also isolates the ground temperature such that it does not change between daytime and nighttime, although it is assumed that the panel shades the ground surface independent of the sun's position in the sky, which is inaccurate but can closely represent dual-axis tracking systems in daytime

cases. During the daytime, the panel overhead the ground surface keeps the ground surface temperature, T_g, cooler than the case with no panel, such that there is a corresponding decrease in mass flux, $\dot{m}''$; the correlation between mass flux and ground temperature is seen in 3.4. Since the panel overhead during nighttime conditions keeps the ground temperature warmer than the case with no panel overhead, this also impacts mass transfer behavior, primarily seen as inhibiting the formation of condensation on the ground surface in some cases, as seen in 3.4, plots [1,0] and [1,2].

During daytime conditions, radiative heat transfer strongly dominates ground surface flux, although the presence of the panel overhead decreases this flux by about 4X, in which convective heat transfer dominates; when convection dominates, the ground conditions no longer depend heavily on irradiation, but wind speed and air temperature. Additionally, with the panel overhead, the convective cooling decreases until T_e approaches the ground temperature, wherein convective flux changes direction and becomes warming with increasing T_e. See 3.2.

Nighttime behavior is similar to daytime, wherein radiation most strongly drives flux with no panel overhead and with the panel present, convection dominates ground surface flux. Both during daytime and nighttime, latent heat transfer increases to compensate for increased convective warming, seen in 3.2 and 3.3 with the panel overhead, as radiative exchange is inhibited.

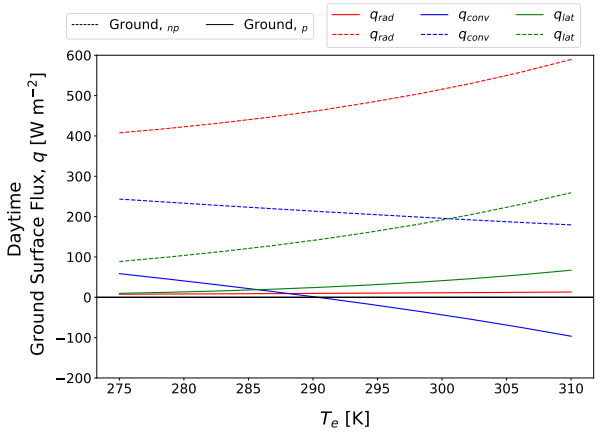

Figure 3.2: Daytime surface fluxes of the ground as a function of T_e, with and without a panel overhead, RH = 0.3, u_e = 3.25 m/s, and ε_g = 0.3.

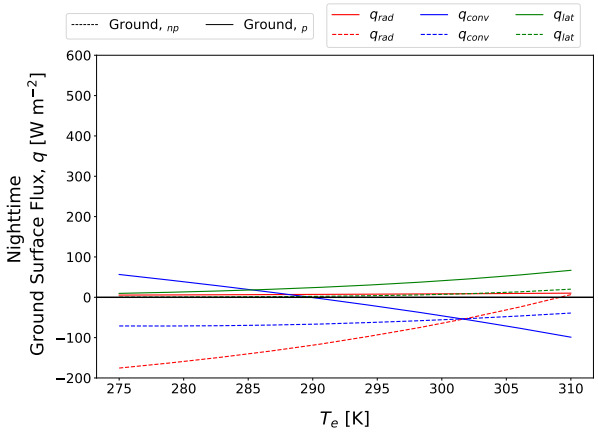

Figure 3.3: Nighttime surface fluxes of the ground as a function of T_e, with and without a panel overhead, RH = 0.3, u_e = 3.25 m/s, and ε_g = 0.3.

Mass flux and ground temperature vary widely as a function of all varied parameters with no panel overhead, the presence of the panel collapses the range of T_g and $\dot{m}''$, shown in 3.4.

Mass flux increases with decreasing ground emissivity, in an open ground-sky interface, as T_g is driven upwards with lack of effective radiation emission. The panel overhead the ground surface removes the dependence of mass flux on emissivity, as it inhibits radiative exchange with the sky. Under nighttime conditions, the presence of the panel inhibits radiative cooling of the ground surface, which ultimately prohibits the formation of condensation on the ground surface over all emissivity values, as seen in 3.4, plot [1,0].

With increasing wind speed, mass flux increases monotonically, in all cases, as expected given increased convective transport which drives the concentration gradient. The panel overhead decreases the sensitivity of mass flux as a function of wind speed during the daytime, given the lack of radiative heating from the sun and sky. See 3.4,

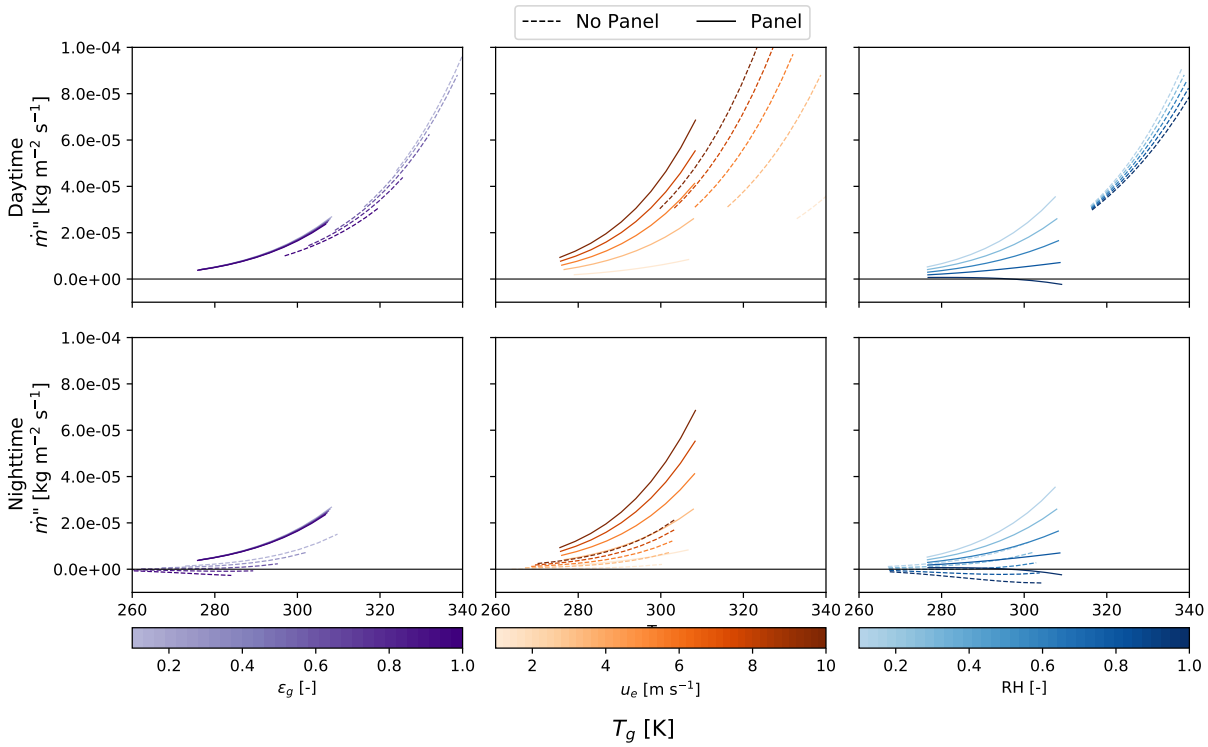

Figure 3.4: Mass transfer rate as a function of ground temperature, under varied parameters: day vs night, ground emissivity, ε_g, wind speed, u_e, and relative humidity, RH. For each parameter varied, the other two are held constant: $\varepsilon_g = 0.3$, $u_e = 3.25$ m/s, and RH $= 0.3$

plots[0,1] and [1,1].

Evaluating $\dot{m}''$ as a function of RH, interestingly shows that the panel allows for condensation to form on the ground surface during the daytime in cases of RH > 0.8; this again is due to the reduced T_g given the lack of radiative heating. Conversely, the ranges of RH which allow formation of dew on the ground surface during the nighttime are impacted; the no panel case shows condensation formation at RH > 0.5, unlike the panel case requiring RH >0.8, which is highly uncommon in desert areas. See 3.4, plots [0,2] and [1,2] for reference.

Looking solely at $\dot{m}''$ as a function of T_e, gives more insight to the sensitivity

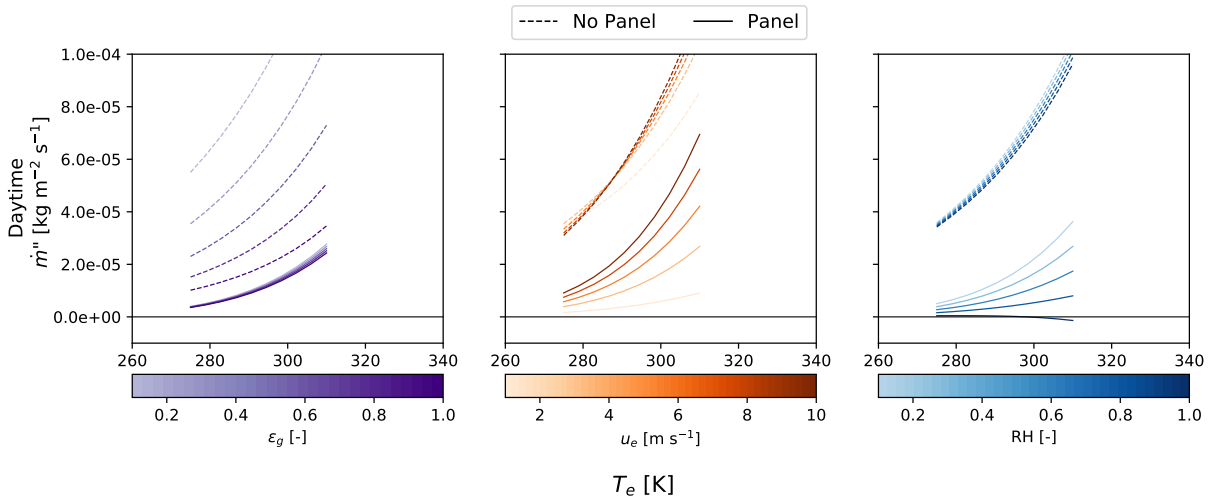

Figure 3.5: Mass transfer rate as a function of air temperature, under varied parameters: day vs night, ground emissivity, ε_g, wind speed, u_e, and relative humidity, RH.

analysis of the varied parameters and their impact to ground surface mass transfer. The open ground-sky interface in all daytime cases show increased mass flux, by almost double in most cases, when compared to the panel overhead. The nighttime results are the same behavior as seen in 3.4, plots [1,0], [1,1], and [1,2]. Ground emissivity is the strongest driving factor for mass flux with no panel overhead, showing a wide range of surface fluxes over varied emissivity. Referencing 3.5, the collapse of the mass flux range in the presence of the panel overhead confirms that ground emissivity is the most impactful parameter to mass flux. The panel overhead removes the ground emissivity dependency and shows that wind speed and relative humidity strongly compete for the largest influence on ground surface mass transfer.

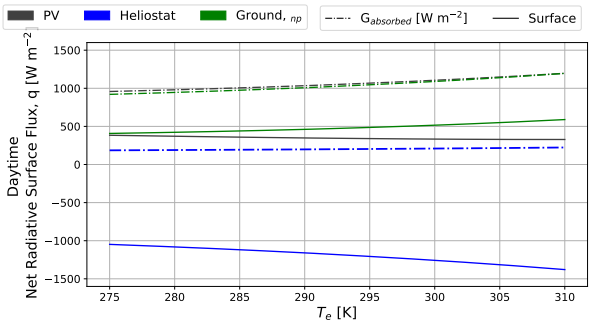

Figure 3.6: Daytime radiative surface fluxes under conditions: RH $= 0.3$, $u_e = 3.25$ m/s, and $\varepsilon_g = 0.3$.

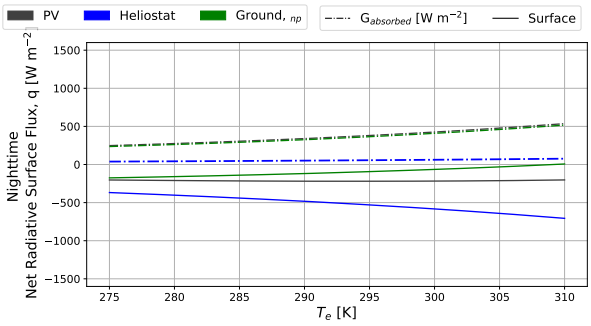

Figure 3.7: Nighttime radiative surface fluxes under conditions: RH $= 0.3$, $u_e = 3.25$ m/s, and $\varepsilon_g = 0.3$.

Lastly, addressing the impact of panel presence on surface albedo, and more specifically, surface flux - it is shown in 3.6 and 3.7 that the PV and heliostat surfaces generate less flux than the ground surface, during both daytime and nighttime conditions. This reduced surface flux changes the overall energy balance for the surface of the Earth relative to the atmosphere, and in some cases quite drastically. The ground and PV panel closely resemble each other, though the PV panel has a lower net flux given it's conversion efficiency and its ability to reject heat on two sides into the air. The heliostat behavior is interesting as it absorbs almost none of the incoming radiation, reflecting most of the incoming radiation back to space, similar to the behavior of snow.

Conclusion

The expansion of USSE demands thorough investigation of the potential impacts to the planet, as well as the electricity market. This paper has given background into the growing scale of USSE, an observed impact known as the Photovoltaic Heat Island effect, and further insight through the modeled results demonstrating the physical manifestations of these concerns at the ground level through ground surface temperature and relative mass transfer rates. Additionally, the surface albedo impacts, shown through surface flux, have been simulated.

The presence of panels, PV or heliostat, show an overall reduction in ground surface temperature and thereby mass flux, during the daytime, locally. Conversely, panels overhead inhibit radiative cooling of the ground surface at nighttime, resulting in higher ground temperatures (seen in data on PVHI, [9], [6]) and subsequently higher mass transfer rates. Under some conditions, there is even an inhibition of dew formation on the ground surface due to the elevated ground temperature. This may be solved with panels being rotated perpendicular to the ground surface during the nighttime, where able. The impact to local wind patterns would likely be affected, effectively increasing surface roughness on a larger scale; this is beyond the scope of this model.

On a larger scale and considering an overall energy balance for the surface of the Earth and the atmosphere, it has been shown that PV panels generate a lower surface flux than the ground, by up to 100 W m^{-2}. PV panels can convert roughly 20% of the incident

shortwave radiation to electricity and can reject heat into the air on two sides, whereas the ground has one interface to reject heat via convection and latent heat transfer and is restricted to conduction at the other face. Heliostat panels reflect almost all incoming energy onto a local fixed point (working fluid or solar collector tower), rejecting the rest, resulting in hundreds of watts of energy leaving the Earth's surface in the shortwave spectrum, and escaping through the atmosphere back to space.

Overall, from a surface energy balance perspective regarding impact on local ground temperature, mass transfer rates, and large-scale surface albedo, the installation and operation of PV panels or heliostats address main concerns around climate change with some benefits. The reduced ground temperature during the day substantially decreases evaporative cooling, thereby keeping water within the Earth's crust; this could impact ground water levels over time, keeping them more stable, as the concentration gradient is reduced at the surface. The loss of evaporation to the sky can impact weather patterns, though the extent is out of the scope of this model. The reduced surface flux of the panels suggest a reduction in the radiative forcing which directly contributes to rising temperature levels of the planet as a whole. Climate models may take these surface changes into account when predicting radiative forcing values.

Appendix

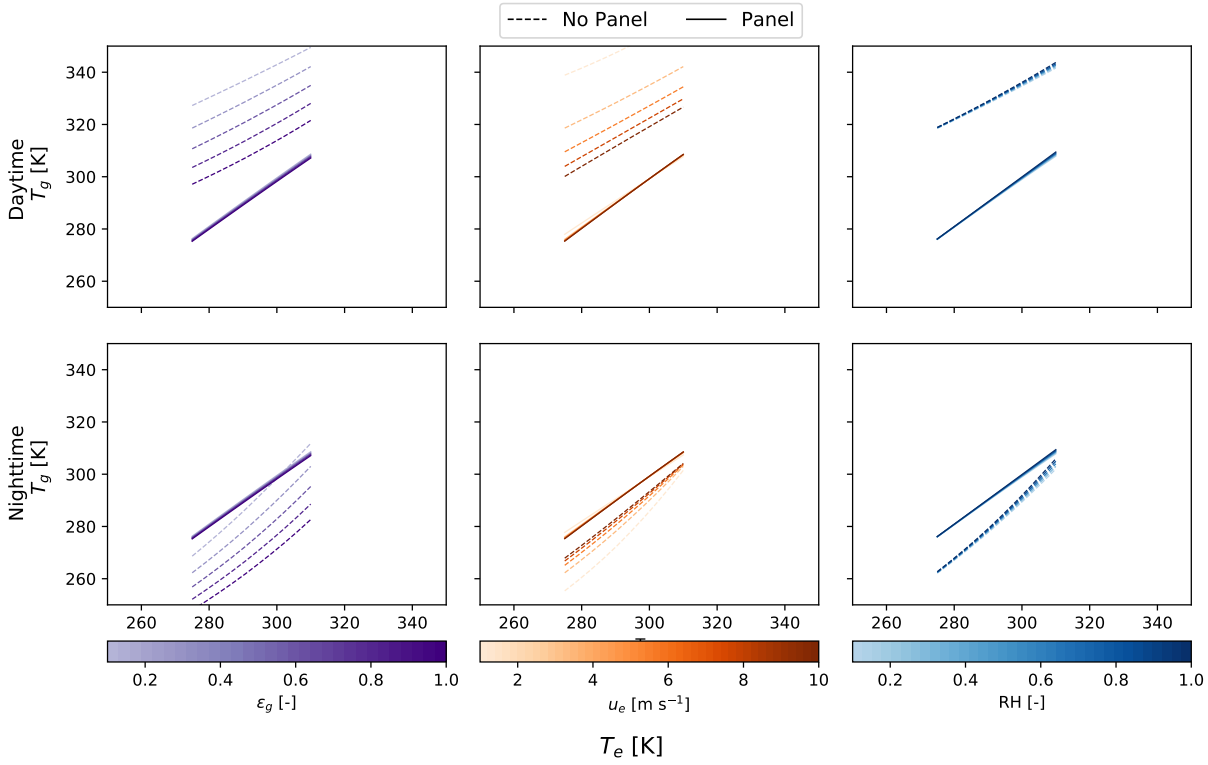

Figure 3.8: T_g as a function of fixed varied range T_e, under varied parameters: ε_g, u_e, and RH.

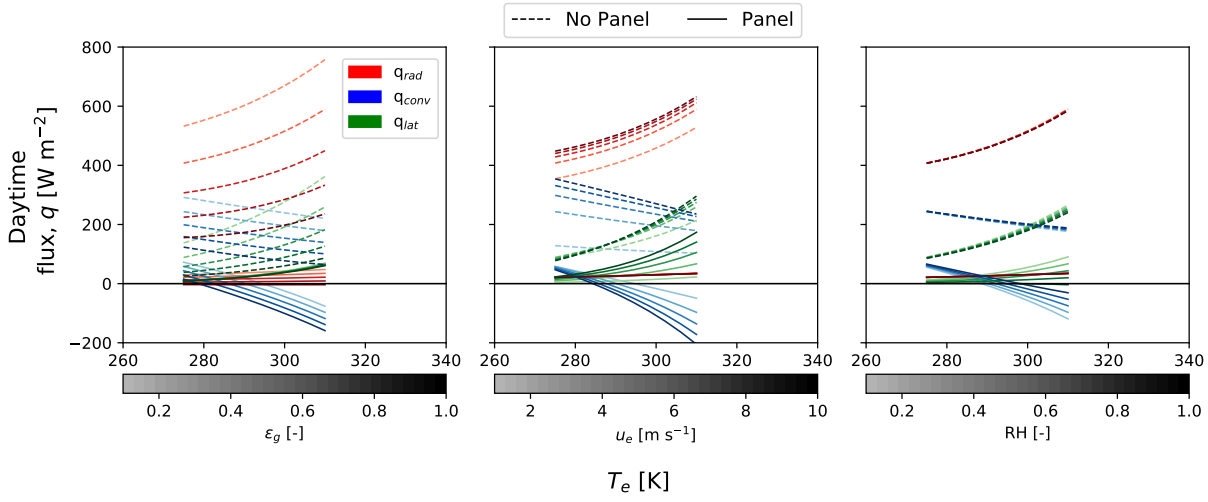

Figure 3.9: Ground surface flux: radiation, convection, latent heat during the daytime under varied parameters: ε_g, u_e, and RH.

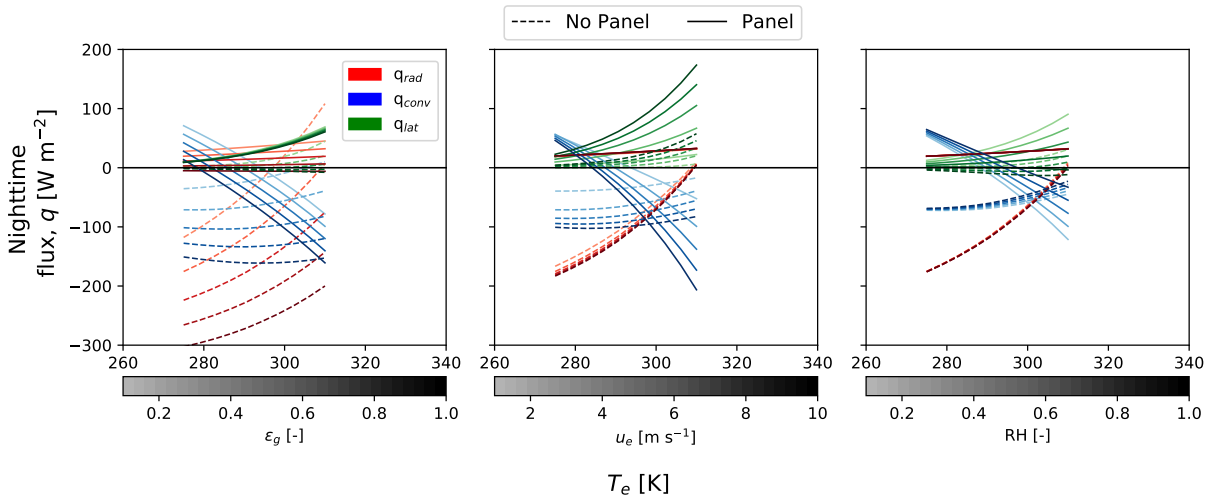

Figure 3.10: Ground surface flux: radiation, convection, latent heat during the nighttime under varied parameters: ε_g, u_e, and RH.

Bibliography

[1] O. Alduchov and R. Eskridge. Improved magnus form approximation of saturation vapor pressure. *Journal of Applied Meteorology*, 35:601–609, 1996.

[2] American Meteorological Society. http://glossary.ametsoc.org/wiki/bowenratio, 06/16/2020.

[3] American Society for Testing and Materials. Reference solar spectral irradiance: Air mass 1.5. https://rredc.nrel.gov/solar//spectra/am1.5/, 04/27/2020.

[4] H. Atwany, M. Attom, M. Hamdan, B. Abu-Nabah, and A. H. Alami. Evaluating thermal conductivity of desert sand under different intial physical properties. *Journal of Advances in Technology and Engineering Research*, 4:236–240, 2018.

[5] Y. Bai, T. Scott, W. C. ad R. Minnich, and A. Chang. Long-term variation in soil temperature of the mojave desert, southwestern usa. *Climate Research*, 46(43 - 50), 2011.

[6] G. Barron-Gafford, R. Minor, A. Brooks, M. Pavao-Zuckerman, and A. Cronin. The photovoltaic heat island effect: Larger solar power plants increase local temperatures (open access: http://www.nature.com/articles/srep35070). *Scientific Reports*, 6:35070, 11 2016.

[7] N. Barth, B. W. Figgis, A. Ennaoui, and S. Ahzi. Field-scale computational fluid dynamics applied to wind velocity profiles of photovoltaic plant: Case of the qeeri solar test facility, doha, qatar. In *2016 International Renewable and Sustainable Energy Conference (IRSEC)*, pages 613–618, 2016.

[8] P. Denholm and M. Hand. Grid flexibility and storage required to achieve very high penetration of variable renewable electricity. *Energy Policy*, 2011.

[9] V. Fthenakis and Y. Yu. Analysis of the potential for a heat island effect in large solar farms. In *2013 IEEE 39th Photovoltaic Specialists Conference (PVSC)*, pages 3362–3366, 2013.

[10] R. Hernandez, S. Easter, M. Murphy, F. Maestre, M. Tavassoli, E. Allen, C. Barrows, J. Belnap, R. Ochoa-Hueso, S. Ravi, and M. Allen. Environmental impact of utility-scale solar. *Renewable and Sustainable Energy Reviews*, 29:766–779, 2014.

[11] A. Hu, S. Levis, G. Meehl, W. Han, W. Washington, K. Oleson, B. van Ruijven, M. He, and W. Strand. Impact of solar panels on global climate. *Nature Climate Change*, 6:290–294, 2015.

[12] J.Lovich and J.Ennen. Wildlife conservation and solar energy development in the desert southwest, united states. *BioScience*, 61(12):982–992, 2011.

[13] M. Li, Y. Jiang, and C. F. M. Coimbra. On the determination of atmospheric longwave irradiance under all-sky conditions. *Solar Energy*, 144:40–48, 2017.

[14] M. Mendelsohn, T. Lowder, and B. Canavan. Utlility-scale concentrating solar power and photovoltaics: A technology and market overview. Technical report, National Renewable Energy Laboratory, 2012.

[15] A. F. Mills and C. F. M. Coimbra. *Basic Heat and Mass Transfer*. Temporal Publishing, San Diego, CA, 3 edition, 2015.

[16] G. Nemet. Net radiative forcing from widespread deployment of photovoltaics. *Environmental Science and Technology*, 43:2173–2178, 2009.

[17] T. R. Oke, G. Mills, A. Christen, and J. A. Voogt. *Urban Climates*. Cambridge University Press, Cambridge, 1 edition, 2017.

[18] H. Ritchie. Renewable energy. *Our World in Data*, 2017. https://ourworldindata.org/renewable-energy.

[19] S.Ong, C.Campbell, P. Denholm, R. Margolis, and G.Heath. Land-use requirements for the solar power plants in the united states. Technical report, National Renewable Energy Laboratory, June 2013.

[20] D. Turney and V. Fthenakis. Environmental impacts from the installation and operation of large-scale solar power plants. *Renewable and Sustainable Energy Reviews*, 15:3261–3270, 2011.

[21] US Energy Information Administration. US electric system operating data. https://www.eia.gov/electricity, 07/10/2020.

[22] Z. Wu, A. Hou, C. CHang, X. Huang, D. Shi, and Z. Wang. Environmental impacts of large-scale csp plants in northwestern china. *Environmental Science: Processes and Impacts*, 16(10):2432–2441, 2014.